*Journal of the Korean Society for Nondestructive Testing*
*Vol. 25, No. 6 (2005. 12)*

# Experimental Analysis of Unsteady Bubble Behaviors Using Three-Dimensional Tomography

Han Seo Ko*,† and Yong-Jae Kim*

**Abstract** Bubble behaviors in a circular tube have been analyzed numerically and experimentally by a three-dimensional tomography method. Initially, a multiplicative algebraic reconstruction technique (MART) which showed better results for previous studies of numerical simulations has been performed to confirm the accuracy of the three-dimensional reconstruction for the two-phase flow using a computer-synthesized phantom. Then, bubble behaviors have been investigated experimentally by the three-dimensional MART method using real projected data captured simultaneously by a laser and three CCD cameras for three angles of view. Also, the transient reconstructions have been attempted to analyze the real-time oxygen-bubble movements in water by the interval of 1/30 second.

**Keywords:** two-phase flow, bubble behavior, multiplicative reconstruction technique, three-dimensional reconstruction, tomography

## 1. Introduction

Gas-liquid two-phase flow is related to phase-change heat transfer and can be shown in many industrial processes such as boilers, condensers, dryers, heat pipes, air conditioners, heat exchangers, etc. Bubbly flows usually appear in the two-phase flow for the case of the relatively low bubble velocity as shown in Fig. 1. As the heat is added more or the velocity of the bubble increases compared with the liquid velocity, the bubbly flow can be changed into the annular flow. Thus, nonintrusive determinations of numbers, locations, and sizes of bubbles are increasingly in demand to measure the component fractions and their distributions for analysis of the two-phase flows. The tomography methods are effective tools of the noninvasive and quantitative measurements of the two-phase flows (Kak and Slaney, 1987).

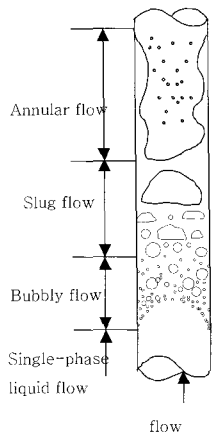


Fig. 1 Schematic of two-phase flow in vertical pipe

The line-of-sight optical projection of the two-phase flow is expressed as a ray integral of the refractive index using an interferometry

Received: September 27, 2005, Accepted: November 2, 2005. * School of Mechanical Engineering, Sungkyunkwan University, Suwon 440-746, † Corresponding author: hanseoko@yurim.skku.ac.kr

(Kihm, 1997, and Partington, 1953) while the projection of a speckle tomography is obtained by the integral of the field density gradient normal to the direction of the incident ray (Francon, 1979, and Ko et al., 2001). The optical projection $\psi_{IF}$ of Mach-Zehnder interferometry is determined by a difference in path length between the reference beam without a phase object and the object beam going through the phase object. The resulting fringe shifts with respect to the undisturbed fringes can be expressed by the ray integration of the density field as follows (Vest, 1979):

$$\psi_{IF} = \frac{1}{\lambda}\int(n - n_{ref})dt = \frac{G}{\lambda}\int(\rho - \rho_{ref})dt \qquad (1)$$

where $\lambda$, $n$, $G$, and $t$ denote the laser wave length, the refractive index, Gladstone-Dale constant, and coordinate parallel to ray direction, respectively. The fringe shift $\Psi_{IF}$ in eqn. (1) must be inverted to reconstruct the true density field $\rho$ and this inversion is called tomography (Ko and Kihm, 1999) for the case of the asymmetric density field.

The tomography methods such as the algebraic reconstruction technique (ART) (Gordon, 1974) and the multiplicative algebraic reconstruction technique (MART) (Verhoeven, 1993) have been carried out to undertake the task of inversion numerically and compared to obtain more accurate and appropriate method for the two-phase flow in the previous study (Ko and Kim, 2003). The MART method which showed better results for the numerical simulation has been developed to reconstruct the three-dimensional bubble behaviors by using a computer-synthesized bubbly flow for limited angles of view in this study. Then, the three-dimensional tomography has been performed experimentally for the unsteady two-phase flow of oxygen-water in the circular tube using optical instruments. Thus, the objective of this study is to develop the simultaneous three-dimensional tomography (MART) instead of stacking up the two-dimensional reconstructions of cross-sections and to investigate the transient bubble behaviors using the developed tomography.

## 2. Tomographic reconstruction algorithm: multiplicative algebraic reconstruction technique (MART)

For a three-dimensional density field, one can represent the field as a series of basis functions allowing their parameters to be optimally determined. The tomography undertakes the optimization task for the linear case where each basis function is defined by a single parameter (usually its unknown height with a fixed spread). The location of each basis function is given as

$$\hat{f}(x,y,z) = \sum_{j=1}^{JKL} O_j b(x - x_j, y - y_j, z - z_j) \qquad (2)$$

where $\hat{f}$ is an object function that represents the field to be reconstructed, $b$ is a general form of the basis function located at $(x_j, y_j, z_j)$, and $G_j$ is the height coefficient of the $j$-th basis function centered at a fixed location of $(x_j, y_j, z_j)$. The $(x_j, y_j, z_j)$ positions form a rectangular array of $J$ equally spaced points in the $x$ direction, $K$ in the $y$ direction, and $L$ in the $z$ direction. Thus, $JKL$ is the total number of coefficients to be estimated by the reconstruction algorithm. The use of a smooth basis function such as a cubic B-spline function can accurately represent a relatively smooth object field with far fewer coefficients (unknowns) than with the square-pixel basis function. An optimized set of these unknowns must be found to minimize the deviations between the virtual projection $\hat{\psi}$ of an intermediate object function $\hat{f}$ and the measured projection $y$ of the actual field $f$.

A comparative study (Hanson and Wecksung, 1985) of the choice of basis functions suggests the use of the cubic B-spline, described in the $x$ variation by

$$b_x(x-x_j)=\begin{cases}\dfrac{\left(2\Delta_x-|x-x_j|\right)^3-4\left(\Delta_x-|x-x_j|\right)^3}{4\Delta_x^3}, & |x-x_j|<\Delta_x\\ \dfrac{\left(2\Delta_x-|x-x_j|\right)^3}{4\Delta_x^3}, & \Delta_x\le|x-x_j|\le 2\Delta_x\\ 0, & |x-x_j|>2\Delta_x\end{cases} \quad (3)$$

where $\Delta$ is the grid spacing. All of the MART results in this research use the cubic B-spline basis function.

The projected ray sum $\Psi_i$ can be obtained as follows:

$$\psi_i=\sum_{j=1}^{JKL}O_j\int_t b\left(x-x_j,y-y_j,z-z_j\right)dt \quad (4)$$

where $i$ = 1, 2, ..., $PQZR$ is the total number of ray sums for the number of equally angled projections in one plane $P$, the number of zenith angles from a horizontal line $Q$, the number of planes in z-direction $Z$, and the number of ray sums per each projection plane $R$. Solving this set of $PQZR$ linear algebraic equations (one equation for each measured ray sum) is the goal of the series-expansion technique such as the MART in $JKL$ unknowns.

The MART algorithm is the basically iterative solver of systems of linear equations (eqn. (4)) adapted to the particular problem of tomographic reconstruction for an object vector $\boldsymbol{O}$. The MART uses the feedback information on the deviation of the virtual projection from the measured projection and iteratively optimizes the object coefficient vector $\boldsymbol{O}$ by an algebraic updating. The MART uses an element $C_j$ of the multiplicative correction vector $C$ as follows:

$$O_j^{q+1}=C_j^qO_j^q$$
$$C_j^q=\begin{cases}1-0.5W_{i,j}^*\left(1-\dfrac{\psi_i}{\hat{\psi}_i}\right), & \hat{\psi}_i\neq 0\\ 1, & \text{otherwise}\end{cases} \quad (5)$$

where $q$ denotes the $q$-th iteration and the normalized weighting factor $W^*_{i,j}$ is equal to $w_{i,j}/w_{max}$ where $w_{max}$ is the largest element of the projection matrix $W$. This algorithm performs the iteration on a ray-by-ray basis until convergence is reached. One advantage of using MART is to ensure a non-negative object field in reconstructing non-negative scalar.

## 3. Computer-Synthesized Phantom and Reconstruction Error

The three-dimensional phantom with three bubbles (Ko and Kim, 2002) has been synthesized and reconstructed numerically before the experimental study. The three-dimensional computer-synthesized phantom as shown in Fig. 2 is expressed by

$$f(x,y,z)=\begin{cases}0, & [(x-0.15)^2+(y-0.15)^2+z^2]^{1/2}\le 0.25\\ 0, & [(x+0.3)^2+(y+0.3)^2+(z+0.1)^2]^{1/2}\le 0.2\\ 0, & [(x-0.1)^2+(y+0.3)^2+(z-0.1)^2]^{1/2}\le 0.15\\ 1, & \text{otherwise}\end{cases} \quad (6)$$

The normalized field impedance is 0 for the region inside the bubble and 1 for liquid outside the bubble.

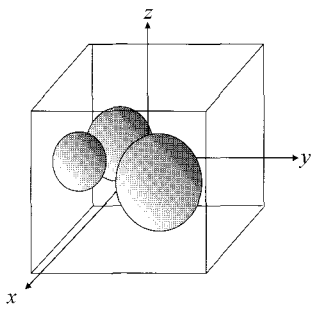


Fig. 2 Computer synthesized three-dimensional two-phase phantom field with three bubbles

The average error of the reconstructed object function $\hat{f}$ and the reference phantom function $f$ is used in this research (Ko et al., 1997):

$$\Phi_{avg}=\frac{\sum_{j=1}^{JKL}\left|f\left(x_j,y_j,z_j\right)-\hat{f}\left(x_j,y_j,z_j\right)\right|}{JKL} \quad (7)$$

where $JKL$ is the total number of the basis functions used to conform to the reconstructing object functions. Note that the average error measures the reconstruction quality based on the comparison between the reconstructed field (object function) and the true field (phantom function). In a real experiment, however, the true field is unknown and the quality of reconstruction is only measured by comparing the virtual projection $\hat{\psi}$ against the measured projection $\psi$.

## 4. Reconstruction of test phantom using MART

The three-dimensional computer-synthesized phantom has been reconstructed numerically before the experimental study. The three-dimensional MART has been developed to calculate the size, shape and location of the bubbles in the two-phase flows. For the case of the three-dimensional reconstruction, more numbers of the projection data are required for the accurate calculation compared with the two-dimensional reconstruction.

The computer-synthesized test phantom has been reconstructed using 3150, 14400, and 15000 rays. Thus, the projection data have been calculated from those rays after assuming the laser beam to be passed through the phantom. For the case of 3150 rays, the reconstruction has been carried out with 3 azimuthal angles for +60°, 0°, and -60° in one plane as shown in Fig. 3 (a) ($P$=3), with 3 and 1 zenith angles from a horizontal line for +60°, 0°, and -60°($Q$=3, 1), with 10 and 30 different heights in $z$-direction ($Z$=10, 30) because of three-dimensional calculation, and with 35 rays for each direction ($R$=35). That is, the total number of rays has been divided into two cases such as

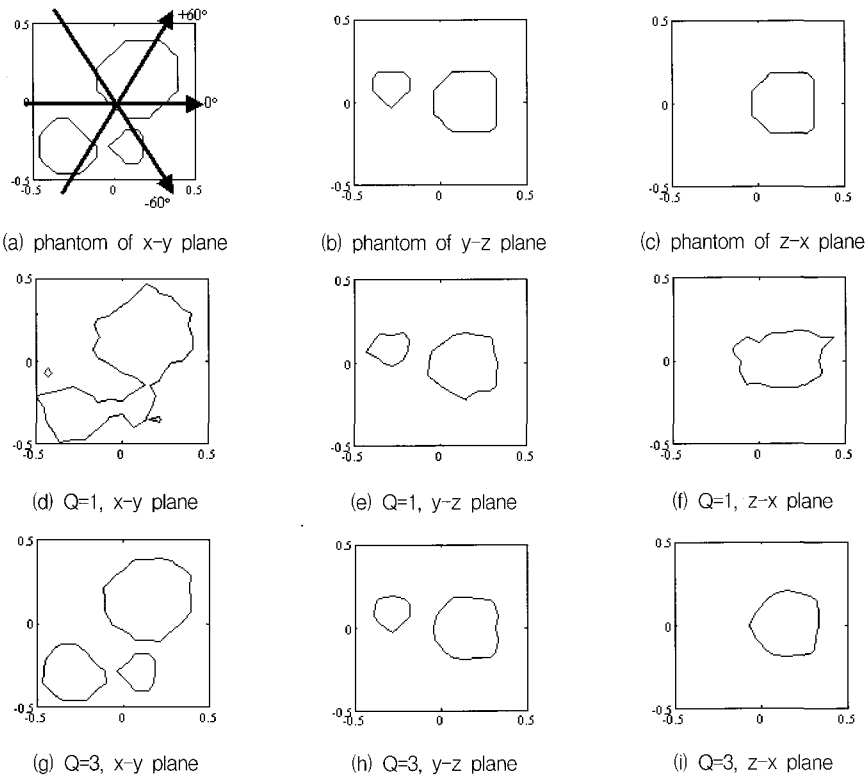


Fig. 3 Reconstructed fields of three-dimensional bubbly flow including three bubbles for 3150 rays

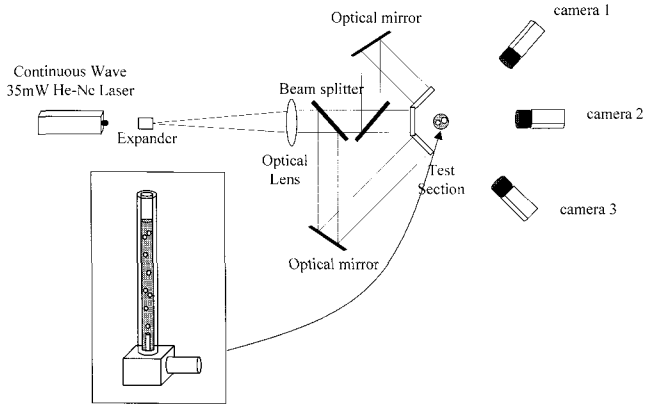


Fig. 4 Experimental setup for visualization of two-phase flow

$P\times Q\times Z\times R=3\times 3\times 10\times 35=3150$ and $P\times Q\times Z\times R=3\times 1\times 30\times 35=3150$ to reconstruct the phantom and compare each other. Then, the total number of rays has been increased to $P\times Q\times Z\times R=3\times 3\times 40\times 40=14400$ and $P\times Q\times Z\times R=3\times 1\times 50\times 100=15000$ to inspect the accuracy of the reconstruction. The number of the basis functions in this study is $15\times 15\times 15=3375$ for the simultaneous three-dimensional reconstruction. The important differences of the three-dimensional reconstruction from compiling the results of the cross-sectional reconstruction are to calculate the density distribution including various heights in $z$-direction simultaneously and to use different zenith angles ($+60^{\circ}$, $0^{\circ}$, and $-60^{\circ}$ from the horizontal line) for the fast and accurate calculation.

The result for 3150 rays has showed that the case of $Q$=3 and $Z$=10 using three different zenith angles gives better reconstruction than that of the case of $Q$=1 and $Z$=30 using more numbers of the different heights as shown in Fig. 3. Although the reconstruction for this case is three-dimensional, the results have been expressed by the center surfaces of the $x$-$y$, $y$-$z$, and $z$-$x$ planes because it is hard to compare the results with the phantom in the three-dimensional field. If the number of the rays increases, the results show better accuracies as confirmed by Table 1. The smaller errors have also been obtained for the case of $Q$=3 as shown in Table 1. Thus, more numbers of the zenith angles from the horizontal line as well as the number of the azimuthal angles in a plane can result in the more accurate reconstructions. However, the acceptable results should be obtained from the small number of projection data for real engineering experiments because of spatial and economical problems, which is one of the objectives for the tomography. Therefore, if the experimental setup for the zenith angles from the

Table 1 Comparison of reconstruction errors using MART for three-dimensional phantom with three bubbles

| PQZR | Number of zenith angle(Q) | $\Phi_{avg}$(%) |
|---|---|---|
| 3×1×30×35=3150 | 1 | 11.56 |
| 3×3×10×35=3150 | 3 | 8.72 |
| 3×1×50×100=15000 | 1 | 1.05 |
| 3×3×40×40=14400 | 3 | 0.18 |

horizontal line is impossible, the acceptable accuracy can be acquired by increasing the numbers of the heights $Z$ in $z$-direction and the azimuthal angles $P$ in one plane.

## 5. Experimental setup

The oxygen bubbles have been produced in the circular and acrylic tube with the inner diameter of 16 mm and the thickness of 2 mm as shown in Fig. 4. The bottom of the tube which filled with water has been connected to an oxygen tank to make oxygen bubbles move upward. The beam from a 35 mW He-Ne laser has been expanded by a 10X beam expander and directed at an optical lens with diameter of 50 mm and focal length of 200 mm to keep the beam width. Then, three projection angles of view has been set up using two beam splitters with 50% of reflectivity and 50% of transmissivity and two optical mirrors with 95% of reflectivity as shown by Fig. 4. Semitransparent screens have been placed in front of the test section to obtain the relatively uniform intensity of the laser beam, which is helpful to distinguish the bubble images from the background images.

The images of moving oxygen bubbles have been captured by three CCD cameras with resolution of 640×480. The captured images have been transferred to a computer by an installed multi-channel capture board. The images of the bubbles have been separated from the whole projected images by an image processing technique to produce the projection data and then the three-dimensional density distributions of the two-phase flow have been reconstructed by the developed three-dimensional tomography method from the projection data.

## 6. Results and discusion

The simultaneous three-dimensional MART has been performed using the projected data from three projection angles of view as shown in Fig. 5 instead of piling up the two-dimensional reconstructions. The number of azimuthal projection angles, planes in $z$-direction, and rays in each projection angle are 3, 42, and 300, respectively. The experiment has not been carried out for various zenith angles because of the spatial problem. Since the reference value does not exist for the experiment, the iteration has been performed until 1000. In this case, the third iteration has showed the best results for the reconstruction of the oxygen bubbles. Thus, the iteration has been ceased at the third one and the density values have been divided into oxygen and water at that iteration.

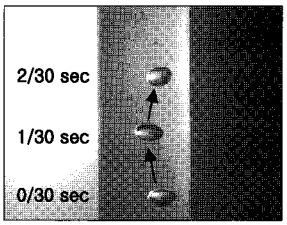


(a) projection #1 (left view)

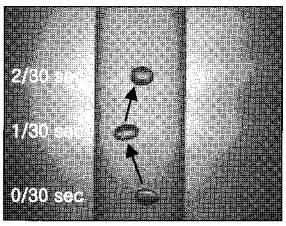


(b) projection #2 (middle view)

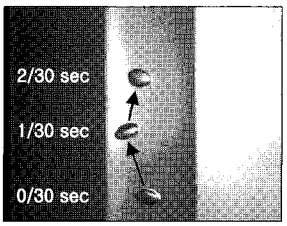


(c) projection #3 (right view)

Fig. 5 Traced image of two-phase flow (oxygen and water)

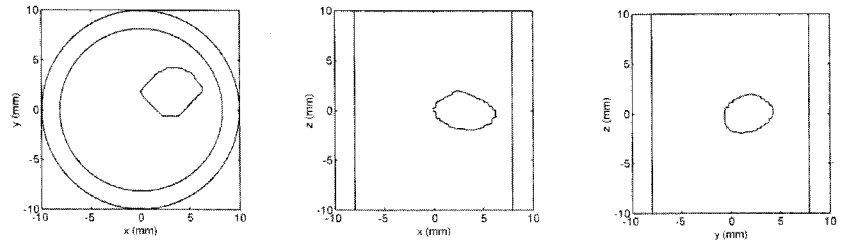


Fig. 6 Reconstructed three-dimensional density distribution at 0/30sec

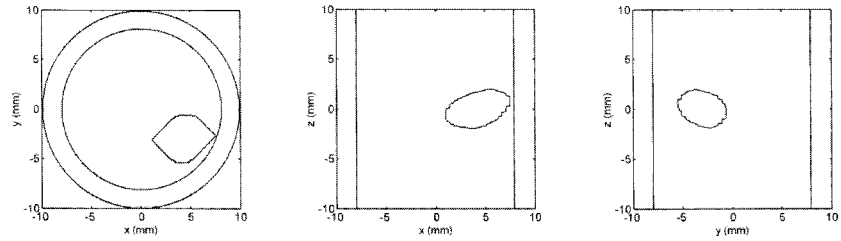


Fig. 7 Reconstructed three-dimensional density distribution at 1/30sec

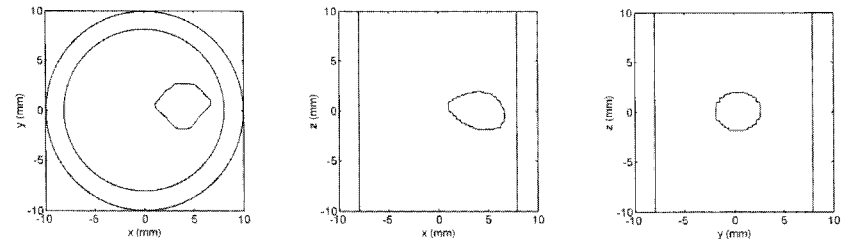


Fig. 8 Reconstructed three-dimensional density distribution at 2/30sec

The projection in this study has been captured from the movie of bubbles with the interval of 1/30 second. Figure 5 shows the combined three bubbles in each projection angle with the interval of 1/30 second. It is observed that the trace of the upward bubble movement is not linear in the circular tube. The simultaneous three-dimensional MART has reconstructed the bubbles as shown in Figs. 6, 7, and 8. The location, shape, and size of the bubble could be reconstructed accurately with time variation by the developed real-time and three-dimensional MART method. The results in *x-z* and *y-z* planes have shown similar shapes of the bubbles as real ones. However, the reconstructed results in *x-y* plane have shown bigger and hexagonal shapes of bubbles compared with real bubbles because three projection angles of view have been used to calculate the results in this case. If more numbers of projection angles can be included in the experiment, more accurate reconstruction can be obtained.

## 7. Conclusions

The three-dimensional MART has been developed to analyze the unsteady oxygen bubble behaviors in the circular tube filled with water. Initially, the MART which showed better results for the two-dimensional reconstructions has been performed to reconstruct the computer-synthesized three-dimensional phantom field with three

bubbles. More accurate and faster results have been obtained for the case of 3 zenith angles by the developed three-dimensional MART.

The developed three-dimensional MART has been applied for the real experiment to calculate the size, location, and shape of the bubbles simultaneously and instantaneously. Although the results in the x-y plane have shown some noise because of the limited angles of view, the simultaneous three-dimensional reconstruction has been accomplished successfully for the unsteady two-phase flows.

## Acknowledgement

This work was supported by the Korea Research Foundation Grant funded by the Korean Government (No. R08-2003-000-10030-0).

## References

Francon, M. (1979) Laser Speckle and Applications in Optics, Academic Press, New York, pp. 120-206

Gordon, R. (1974) A Tutorial on ART, IEEE Trans. on Nuclear Science, Vol. NS-21 pp. 78-92

Hanson, K. M. and Wecksung, G. W. (1985) Local Basis Function Approach to Computed Tomography, Appl. Opt., Vol. 24, No. 23, pp. 4028-4039

Kak, A. C. and Slaney, M. (1987) Principles of Computerized Tomographic Imaging, IEEE Press, New York, USA, pp. 49-112

Kihm, K. D. (1997) Laser Speckle Photography Technique Applied for Heat and Mass Transfer Problems, Advan. in Heat Transfer, Vol. 30, pp. 255-311

Ko, H. S. and Kihm, K. D. (1999) An Extended Algebraic Reconstruction Technique (ART) for Density-Gradient Projections : Laser Speckle Photographic Tomography, Exper. Fluids, Vol. 27, No. 6, pp. 542-550

Ko, H. S. and Kim, Y. -J. (2002) Comparison and Analysis of Tomography Methods for Reconstruction of Three-dimensional Density Distributions in Two-phase Flows, Journal of the Korean Society for Nondestructive Testing, Vol. 22, No. 5, pp. 545-556

Ko, H. S. and Kim, Y. -J. (2003) Tomographic Reconstruction of Two-Phase Flows, KSME International Journal, Vol. 17, No. 4, pp. 571-580

Ko, H. S., Lyons, D. P., and Kihm, K. D. (1997) A Comparative Study of Algebraic Reconstruction (ART) and Genetic Algorithms (GA) for Beam Deflection Tomography, ASME Fluids Engrg. Div. Summer Meeting, Vancouver, Canada, Paper FEDSM 97-3104

Ko, H. S., Okamoto, K., and Madarame, H. (2001) Reconstruction of Transient Three-dimensional Density Distributions Using Digital Speckle Tomography, Meas. Sci. Tech., Vol. 12, No. 8, pp. 1219-1226

Partington, J. R. (1953) Physico-Chemical Optics, Vol. IV, An Advanced Treatise on Physical Chemistry, Longmans Green, London, pp. 314-378

Verhoeven, D. (1993) Limited-data Computed Tomography Algorithms for the Physical Sciences, Appl. Opt., Vol. 32, No. 20, pp. 3736-3754

Vest, C. M. (1979) Holographic Interferometry, John Wiley & Sons, New York, USA, pp. 64-103